Trainable WEKA Phase Segmentation on SEM/BSE Images of Slag Blended Cement Pastes

Natalia M. Alderete[1,2], Yury A. Villagrán Zaccardi[1,2] and De Belie Nele[1]

[1]Labo Magnel, Ghent University, Tech Lane Ghent Science Park, Campus A, Technologiepark Zwijnaarde 904, B-9052 Gent, Belgium

[2]LEMIT and CONICET, 52 entre 121 y 122 s/n, 1900 La Plata, Argentina

ABSTRACT

Scanning electron microscopy with backscattered electrons (SEM/BSE) is a powerful technique that allows the visualization of polished cross sections with good reproducibility and level of detail. It is widely used to study the microstructure of cement-based materials and identify different phases in the cement paste. However, in some cases it is difficult to distinguish between some phases due to a similar grey level, as in the case of slag and portlandite. Then, X-ray elements mapping is necessary to help in the differentiation according to composition, but it can be quite time consuming and tedious with standard detectors. A machine learning tool, trainable WEKA segmentation (TWS), can be used to train a classifier by means of pixel grey values and segment the different phases automatically without any assistance of compositional mapping, transforming the problem into a pixel classification issue. The trained models can be improved by adjusting each class. The application of the model to the images results in a segmented image that can be used for quantification. In this paper TWS is applied for segmenting SEM/BSE images without the need of elements mapping. Slag blended cement pastes at different ages are studied. Results are compared with image analysis through elements mapping and selective dissolution. From this comparison, some information regarding the image density of the portlandite is derived.

Keywords: Image analysis, trainable WEKA segmentation, phases, slag, portlandite

1 INTRODUCTION

Image segmentation is a powerful tool to separate sections of interest for image analysis. The main challenge of this technique is to obtain a reliable set of features that represent each segmented section/phase of the image. To deal with this task several approaches have been developed, as graph-based methods, region merging techniques, mapping image pixels to some feature space, etcetera. A review on image segmentation methods can be found in [1]. Particularly the waikato environment for knowledge analysis (WEKA) project aims to provide a comprehensive collection of machine learning algorithms and data processing tools to researchers and practitioners alike, and its workbench includes algorithms for image classification [2]. Trainable WEKA segmentation (TWS) is a plug-in, included in free

licensed Fiji environment that combines a collection of machine learning algorithms with a set of selected image features to produce pixel-based segmentations [3]. The image segmentation by pixel classification is based on the fact that all images are composed by pixels which are represented by a numeric value. A set of input pixels that are manually labelled into a specific class is later used as the training set for a selected classifier (algorithm that implements classification). The critical issue lies in an accurate segmentation of the images, but as TWS works interactively, adjustment of the model can be made after each training. The trained models (classifiers and clusters) can be improved by adjusting each class, as necessary, to achieve a good segmented image.

Once the classifier is trained, it can be used to classify either the rest of the input pixels or a completely new image automatically [3]. The defined model is then applied to the rest of the images, and a segmented image is one of the outputs. This machine learning tool has already been successfully used for different purposes, such as quantification of reactive oxygen species [4], prediction of solar radiation [5], monitoring the population of solitary bees [6]. Its strength relies on the ability to solve supervised and unsupervised learning problems based on a user defined number of image features.

Scanning electron microscopy with backscattered electrons (SEM/BSE) is a powerful technique that can be applied for the visualization of polished cross sections with good reproducibility and level of detail. Images from SEM/BSE are a widely used to study cement pastes [7]. One of the main reasons for this is that from SEM/BSE images it is possible to quantify, by image analysis, different constituents. However, for pastes with some supplementary cementitious materials (SCMs), additional information may be required from elemental (energy-dispersive X-ray spectroscopy) EDS mapping to achieve a reliable analysis. For the case of slag, SEM/BSE images may be combined with Mg maps to distinguish the slag from the portlandite, due to a similar grey level. Then, X-ray elements mapping is necessary to help in the differentiation according to composition, but this can be quite time consuming and tedious with standard detectors. Good resolution normally requires an image acquisition time of up to 10 h [8].

The aim of this work is to introduce a machine learning tool, TWS, to cement paste image analysis. SEM/BSE images of pastes with slag at four different hydration ages were analysed. TWS was used to segment five classes (Portlandite “CH”, slag particles “Slag”, calcium silicate hydrate “CSH”, anhydrous cement “Cement”, and pores “Pores”) by means of a training set for a selected classifier. Results were compared with two other independent techniques: selective dissolution (SD) and segmentation from EDS mapping, to validate the models. Furthermore, an estimation of the evolution of CH image density could be made considering the results from TWS and thermogravimetric analysis (TGA).

2 MATERIALS, SAMPLE PREPARATION AND SEM/BSE IMAGES ACQUISITON

Ordinary Portland cement was used to prepare the pastes with a water/binder (*w/b*) ratio of 0.4, and a 40 wt.% slag. Dry materials were first homogenized and then mixed with tap water using a laboratory mixer at 1600 rpm. Cylindrical moulds of 33 mm in diameter were used to cast the pastes and seal-cure them for 1, 7, 28, and 90 days.

From the cylinders, discs of approximately 2.5 mm in thickness were cut and kept immersed in isopropanol for 7 days to stop the hydration (with replacement at 1 and 3 days).

The discs were then kept in vacuum desiccators for 7 days to remove the isopropanol. Epoxy-impregnated paste discs were polished and coated with a 15 nm conductive carbon layer for SEM/BSE image analysis.

The SEM/BSE images were acquired at a magnification of 400x. Each image consists of 1280 x 1024 pixels which corresponds to a total area of 305 x 228 μm^2. A mean of 13 images were taken from each sample.

An EDTA extraction method was used for SD, following the guidelines provided in [9]. The consumption of portlandite was measured by TGA in accordance with the guiding principles described in [10].

3 DEVELOPING A MACHINE LEARNING TOOL FOR SEM/BSE IMAGES

3.1 Model generation

As mentioned before, for the model generation TWS uses machine learning algorithms and image features to produce segmentations. Descriptions and possible settings of each step can be found in [11]. In this work, to allow phase identification, it was decided to distinguish among five classes: CH, Slag, CSH, Cement and Pores. Some traces were input to each class to characterize them and then normally the classifier could be trained for all images. However, since grey levels for the same class were different from age to age, if a single classifier model were created for all ages, the trained classifier would account different features at different ages. To ensure reliability in the results, images were divided in groups corresponding to each age (1d, 7d, 28d, and 90d). Then, one image of each group was used to build up the corresponding model and train the corresponding classifiers.

After each model was created, images from the corresponding group were segmented into classified images. Furthermore, based on the applied model, the probability that each pixel belongs to each class can be displayed on a 32-bit hyperstack. Then, probability maps in grey scale for each class are obtained with values between 1-white (100% chance the pixel belongs to that class) and 0-black (0% chance the pixel belongs to that class). These probability maps are particularly important since they give the user the freedom to define the level of confidence desired for each data set. They also show graphically the probability distribution of each class. Additionally, it is possible to generate a receiver operating characteristic (ROC) graph, which allows the visualization, organization and selection of classifiers based on their performance [10]. A scheme of the described steps for the model generation, application and evaluation is shown in Figure 1.

3.2 Relative area amount for the different classes

As mentioned before, TWS provides the probability of each pixel to correspond to a particular class. Then the amount of pixels that belong to each class can be quantified by means of a histogram with a certain probability level. It is important to mention that a particular pixel could have high probabilities of belonging to more than one class simultaneously, depending of the outcome of the classifier. Consequently, the sum of the areas for all phases may not correspond to the total amount of pixels. The relative amount of pixels belonging to each group reflects the relative area of each phase. In principle, a 75% of probability of each pixel belonging to a particular class was chosen as an acceptable limit. Choosing a higher value than 75% can lead to disregard a sensitive amount of information; on

the other hand, choosing a lower value would lead to a higher value of uncertainty. However, it should be noticed that when selecting the 75% level of probability, certain features with low probability of belonging to any class are left out of the counting. This leads to slight underestimations of constituents since not all pixels are considered.

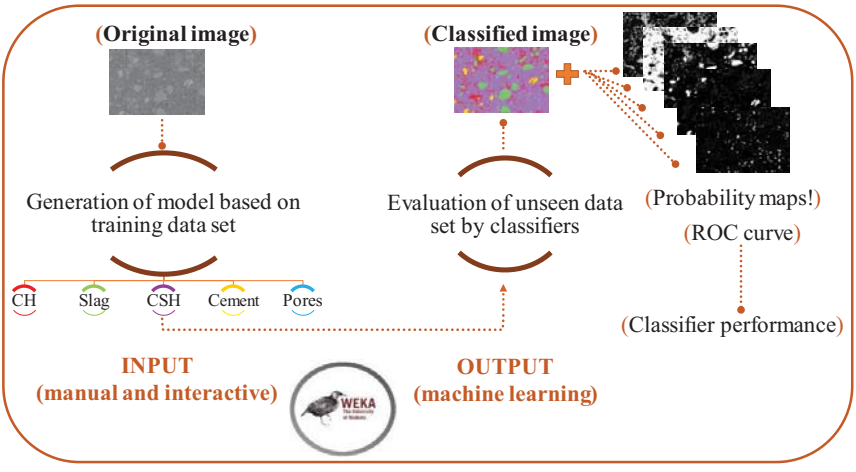

Figure 1: Scheme of steps for the model generation, application and evaluation

One way to address the underestimation issue is to increase the amount of pixels considered for the quantification, including pixels with 70% or 60% probability of belonging to a particular class, although in this case some features may be counted in erroneous classes and precision would certainly decrease. Another method could be to scale the number of pixels per class to sum the total amount of pixels in the image, i.e., transform results to their equivalent 100%. Although, this would imply the assumption that all classes increase linearly with the increase in probability, which may not be the case. For cement paste SEM/BSE images, some phases are certainly more homogeneous than others and therefore they are harder to be accounted for when having a more spread probability distribution.

The distribution of probability of each class was considered to determine which classes have the highest precision (and can be considered with 95% of probability) and which classes should be considered at 75% to include the most of the information possible. Figure 2 shows the probability distribution of each class for a classified image at 1 day of hydration. It was observed that Cement, Pores and CH are the classes with the highest precision, although CH is less precise than slag in relative terms. Arrows ‘a’ and ‘b’ point to the curves from CSH and Slag, which still comprise pixels below 95%. Then, for those two classes, the relative amount obtained at 75% was transformed into the equivalent 100%, to account for the not included data. For the other classes, the precision of each class was enough to consider the pixels at 95% of probability.

This approach shows that the level of probability has to be decided on a probability distribution basis. A high level of probability may be chosen (95% for example) for all classes if none of them has a marked curve after that level. If a verification of such curves is not made, important data could be left out of the quantifications.

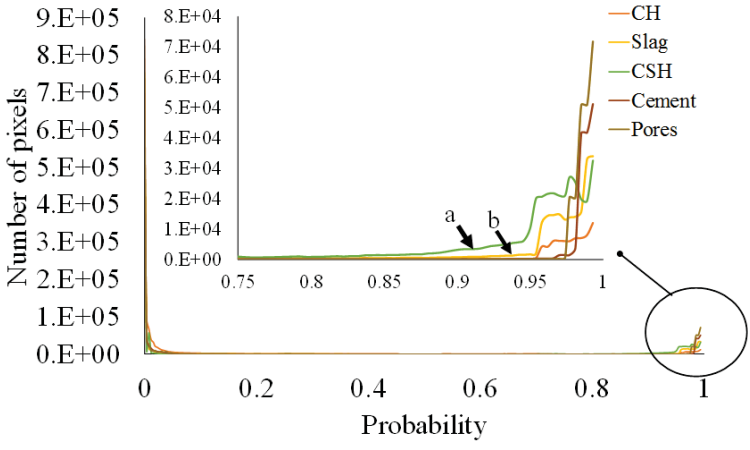

Figure 2: Probability distribution of each class

Figure 3 shows the results of the four models (1d, 7d, 28d, and 90d) quantified as relative amount of area for each class, considering the corrections mentioned above. Variation of phases with time show the progress in the reaction of the slag used.

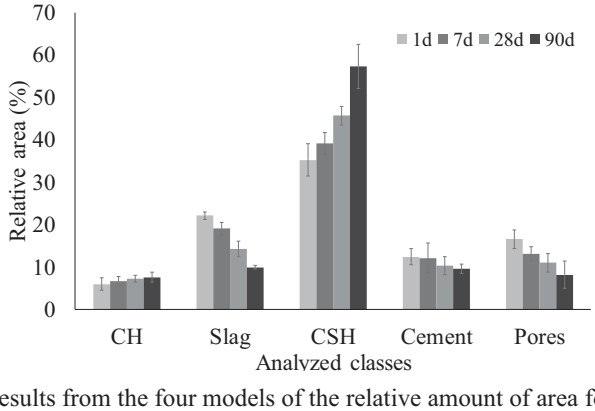

Figure 3: Results from the four models of the relative amount of area for each class

4 COMPARISONS WITH OTHER EXPERIMENTAL TECHNIQUES AND DISCUSSIONS

4.1 Quantification of slag by TWS compared with selective dissolution and SEM mapping results

In order to validate the results from the segmentation, comparisons were made of the quantified amounts of slag with other techniques. Figure 4 shows the correlations between the

amount of unreacted slag quantified by selective dissolution (in blue squares) and the amount quantified by SEM images based on EDS full element maps (red circles) compared with TWS results. A good correlation is observed in both cases, however, it seems that TWS generally overestimates the amount of slag in comparison with both techniques, or that slag content is underestimated with those techniques. For SEM/BSE mapping, previous studies have shown that underestimation is possible on the basis of difficulties to account for the smallest slag particles [12]. However, especially for the case of selective dissolution, results at 1 day are particularly higher than results from TWS or SEM mapping. This may be attributed to incomplete correction procedure of the dissolved part of slag and the undissolved aluminosilicate hydrates [13].

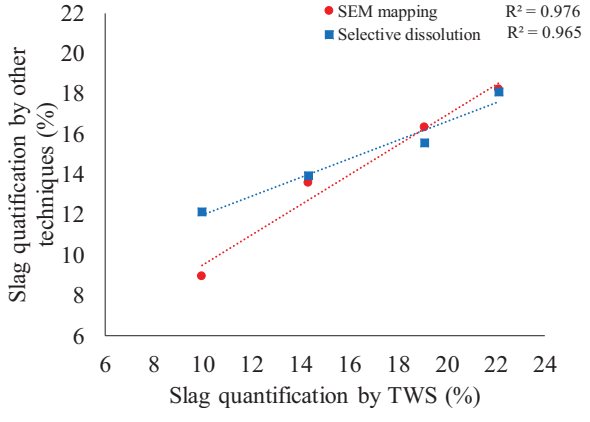

Figure 4: Correlation between amounts of unreacted slag obtained by TWS and other techniques

4.2 Estimation of CH image density

In theory, the stereology principles state that area fractions in 2D cross-sections are equal to 3D volume fractions [14]. Although, 2D cross-sections tend to be underestimated and 2D thickness of features tend to be overestimated [15]. This issue, however, is overcome with enough data from a fairly large representative area. Then, results for relative area of each class from TWS are equal to their volume fraction in the paste. Thus they can be expressed in cm^3 per 100 cm^3 of paste. Based on the CH relative volume and the TGA data (% expressed in weight), results were used to estimate the CH image density and its variation with time considering the measured density of the paste at different ages. Calculations lead to a relation between the density of the CH and the density of the paste as shown in Equation 1. Therefore, with the data from TWS, the image density of the CH can be estimated at different ages. Figure 5 shows (a) the correlation factor found between the density of the paste and the image density of the CH, and (b) the evolution with time of the CH image density calculated with the described method. These values are naturally lower than the density of calcium hydroxide crystals. They cannot account for the actual density of the phase, but only serve as a relationship between the mass and the area observed in the image, named in this case "image density".

$$\frac{\text{TGA results}}{\text{TWS results}} = \frac{\frac{g_{CH}}{g_{paste}}}{\frac{cm^3{}_{CH}}{cm^3{}_{paste}}} = \frac{(g_{CH}) \cdot [cm^3{}_{paste}\ ]}{(cm^3{}_{CH}) \cdot [g_{paste}]} = \frac{\rho_{CH}}{\rho_{paste}} = \quad \text{a (1)}$$

Then: $\rho_{CH} = a \cdot \rho_{paste}$

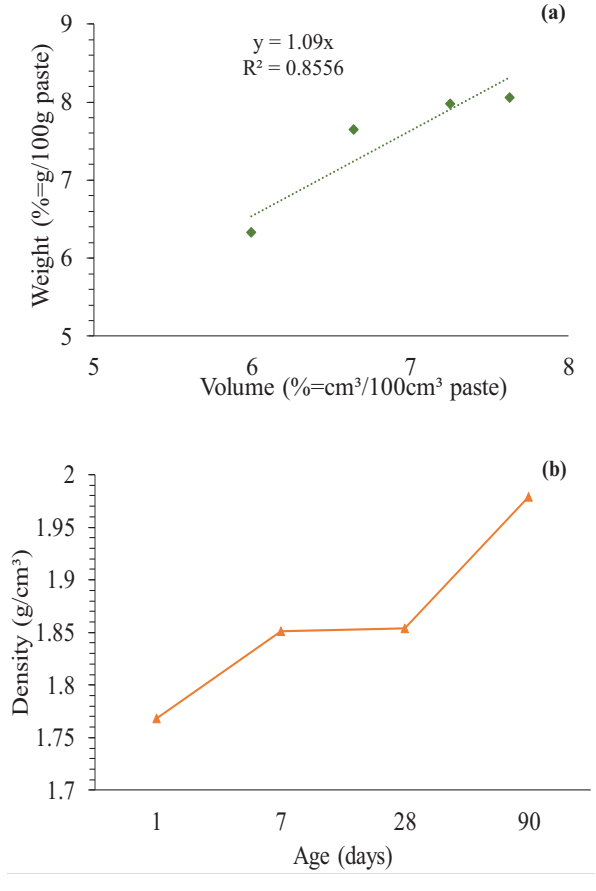

Figure 5: (a) Correlation factor between the density of the paste and the image density of the CH, (b) evolution with time of the CH image density

In theory, the density of the of CH is 2.25g/cm^3 [16]. Although, the density of CH measured on a white cement paste of 0.5 *w/b* at 21 days using ptychographic X-ray computed tomography was found to be of 2.12 ± 0.06 g/cm^3 [17]. The authors attributed this lower-than-expected density to porosity below the spatial resolution and to partial decalcification of the

calcium hydroxide due to the carbonation. The estimation of the image density using the TWS data gives a value of 1.98 g/cm^3 for a slag-blended paste at 90 days. In spite the low value, it was possible to estimate the progress of the CH densification as a function of time.

5 CONCLUSIONS

- A machine learning tool, TWS, was introduced to slag blended cement paste image analysis. It was found to be a useful tool for images segmentation, without the need of element mapping for the distinction among phases.
- When obtaining the probability maps form each designed class, attention should be paid to the chosen level of probability of the different trained classes. It is necessary to assess the probability distribution to identify the precision of each classifier in order not to disregard significant data.
- Validation of the results was made with two other independent techniques: selective dissolution and SEM/BSE mapping. TWS showed a good correlation with both techniques, especially with SEM/BSE mapping. In this sense, it implies significant reduction of time for image acquisition when no mapping is required.
- The potential of TWS has also been shown through the estimation of the CH content and its evolution with time. Although more work is necessary to link the CH image density to the physical density in structure of the paste, the TWS technique shows potential for the evaluation of the density of the constituents of cement pastes.

6 REFERENCES

[1] Pal N. and Pal S., 'A review on image segmentation techniques', *Pattern Recognition* **26** (9) (1993) 1277-1294.

[2] M. Hall, E. Frank, G. Holmes, B. Pfahringer, P. Reutemann, I.H. Witten, The WEKA data mining software: an update, SIGKDD Explorations 11 (2009) 10–18.

[3] Arganda-Carreras, I., Kaynig, V., Rueden, C., Schindelin, J., Cardona, A., Seung, H., 'Trainable_Segmentation: Release v3.1.2 [Data set] ', Zenodo (2016) http://doi.org/10.5281/zenodo.59290

[4] Sekulska-Nalewajko J., Gocławski J., Chojak-Kozniewska J., Kuzniak E., 'Automated image analysis for quantification of reactive oxygen species in plant leaves', *Methods* **109** (2016) 114–122.

[5] Yadav A., Malik H., Chandel S., 'Selection of most relevant input parameters using WEKA for artificial neural network based solar radiation prediction models', *Renewable and Sustainable Energy Reviews* **31** (2014) 509–519.

[6] Hart N. and Huang L., 'Monitoring populations of solitary bees using image processing techniques', *Int. J. Computer Applications in Technology* **50** (1) (2014) 45-50.

[7] Scrivener K., Bazzoni A., Mota B., Rossen E., 'A Practical Guide to Microstructural Analysis of Cementitious Materials' *CRC Press* (2015) 351–418 (Taylor & Francis Group, Boca Raton, 2016)

[8] Kocaba V., Gallucci E., Scrivener K., 'Methods for determination of degree of reaction of slag in blended cement paste' *Cem. Concr. Res.* **42** (2012) 511-525

[9] Lumley J., Gollop R., Moir G., Taylor H., 'Degrees of reaction of the slag in some blends with Portland cements', *Cem. Concr. Res.* **26** (1996) 139–151.

[10] Durdziński1 et al., 'Outcomes of the RILEM round robin on degree of reaction of slag and fly ash in blended cements' (2017), in preparation.